

CMOS Neurostimulation ASIC with 100 Channels, Scaleable Output, and Bidirectional Radio-Frequency Telemetry

Gregg Jørgen Suaning and Nigel H. Lovell*, *Senior Member, IEEE*

Abstract—100-channel neurostimulation circuit comprising a complementary metal oxide semiconductor (CMOS), application-specific integrated circuit (ASIC) has been designed, constructed and tested.

The ASIC forms a significant milestone and an integral component of a 100-electrode neurostimulation system being developed by the authors. The system comprises an externally worn transmitter and a body implantable stimulator. The purpose of the system is to communicate both data and power across tissue via radio-frequency (RF) telemetry such that externally programmable, constant current, charge balanced, biphasic stimuli may be delivered to neural tissue at 100 unique sites.

An intrinsic reverse telemetry feature of the ASIC has been designed such that information pertaining to the device function, reconstruction of the stimulation voltage waveform, and the measurement of impedance may be obtained through noninvasive means.

To compensate for the paucity of data pertaining to the stimulation thresholds necessary in evoking a physiological response, the ASIC has been designed with scaleable current output.

The ASIC has been designed primarily as a treatment of degenerative disorders of the retina whereby the 100 channels are to be utilized in the delivery of a pattern of stimuli of varying intensity and or duty cycle to the surviving neural tissue of the retina. However, it is conceivable that other fields of neurostimulation such as cochlear prosthetics and functional electronic stimulation may benefit from the employment of the system.

Index Terms—Neurostimulator, retina, telemetry, vision prosthesis, VLSI.

I. INTRODUCTION

RECENT and promising progress toward the treatment of retinal disorders such as retinitis pigmentosa and macular degeneration through electronic stimulation of surviving retinal tissue is being made by a handful of research centers [1]. With a variety of innovative technological approaches being attempted, the profound blindness associated with these degenerative diseases may soon become treatable.

The University of New South Wales' (UNSW) vision prosthesis project draws upon some of the concepts utilized in the

implementation of cochlear prostheses that have been extremely successful in the treatment of profound and severe deafness. Varying these concepts so as to derive a prosthesis suitable for stimulation of the visual pathway, the authors have developed a complementary metal oxide semiconductor (CMOS) application-specific integrated circuit (ASIC) that is capable of supplying externally programmable, constant current, charge balanced, biphasic stimulus to 100 unique electrode sites.

Successful treatment of the effects of retinal diseases through neural stimulation requires that the neural pathway between the stimulation site and the appropriate sectors of the brain remain intact.

Recent studies by Veraart *et al.* have led to renewed optimism that stimulation of the optic nerve may be capable of conveying spatially mapped patterns to patients fitted with a cuff electrode upon their optic nerve attached to a stimulation circuit [2].

The retina, because of its accessibility with established surgical techniques and its well-defined topographic mapping of visual space, may be the most appropriate site for the placement of a stimulating apparatus when physiologically excitable neurons survive. Researchers at Johns Hopkins University (Baltimore, MD) have confirmed that in the macular region, human retinal ganglion cells maintain their viability long after the onset of certain forms of blindness [3] but to a lesser extent in the extra-macular region [4]. The authors intend for the 100-electrode sites to be used to form a mapped pattern or image by varying either the stimulus intensity or duty cycle (or both) delivered to each of the electrodes mounted on the surface of the retina. As programming of the stimuli is performed externally, any number of processing and stimulation strategies may be applied to optimize the input to the patient.

In order to avoid the necessity of passing wires through tissue, data and power for the ASIC and its peripheral components are passed through tissue via radio-frequency (RF) telemetry. The RF configuration data is delivered from the external transmitter in accordance with a strict protocol. Violations of this protocol place the ASIC into an error state such that it is reset and awaits valid data. This serves to prevent erroneous RF data from causing the delivery of potentially painful or harmful stimuli to the retinal tissue.

Chronic implantation of such a device in humans would serve as an embryonic step in an ongoing endeavor to provide useful photic input to the blind. Successful implantation would also provide an opportunity to study the psychophysical and physiological effects of chronic neurostimulation of the visual pathway. *In situ* assessment of these effects would be greatly

Manuscript received August 16, 1999; revised October 9, 2000. This work was supported by the Australian Federal Government under a Grant from the Cooperative Research Centres Programme, and by the Clive and Vera Ramaciotti Foundation. *Asterisk indicates corresponding author.*

G. J. Suaning is with the Graduate School of Biomedical Engineering and the Department of Ophthalmology, University of New South Wales, Sydney, Australia, 2052.

*N. H. Lovell is with the Graduate School of Biomedical Engineering, University of New South Wales, Sydney, Australia, 2052 (e-mail: N.Lovell@unsw.edu.au).

Publisher Item Identifier S 0018-9294(01)00576-6.

enhanced by the ability to query the implanted electronics and obtain data pertaining to the voltage waveform across the stimulation circuit without the need for invasive recording probes. To address this issue, a “reverse telemetry” feature has been designed into the ASIC so that the end-of-phase voltage across the neural tissue may be measured.

One-hundred electrodes, while likely to be capable of delivering only rudimentary images, may offer patients significant life enhancing treatment to blindness [5] and will serve as a basis from which future designs may be developed.

A prototype of the circuit described here was first constructed and tested using discrete components [5]. The description of the CMOS ASIC serves as the next step in the evolution of the UNSW vision prosthesis.

A. State of the Art in Retinal Prostheses

Over the years, some researchers have sought to stimulate the retina electrically. Brindley’s 1955 studies [6] identified the parameters necessary to evoke a psychophysical response in humans. More recent studies by researchers at Johns Hopkins University [7] have shown that stimulation of the epiretinal surface can deliver the perception of light in patients blinded by degenerative diseases of the retina such as retinitis pigmentosa and macular degeneration. Subretinal stimulation studies in the rabbit by Chow [8] indicate that the subretinal surface may also be an appropriate site. The optimal location for neurostimulation of the retina remains a topic of intense debate and thus, present day activities in the development of stimulating prostheses for the retina may be divided into two classifications: subretinal and epiretinal stimulation. These classifications are based upon the placement of the stimulating electrodes within the ocular anatomy.

Subretinal proposals include those by Chow and his co-workers of Loyola University (Chicago, IL) [9] and Zrenner’s team at the University of Tübingen, Germany [10]. These proposals primarily consist of photodiode circuitry with stimulating electrodes placed beneath the retina at the retino-pigment epithelium interface. Prostheses of this nature possess several attractive attributes, most significantly their use of direct incident light to derive power and deliver stimuli. Furthermore, this approach is able to provide high quantities of stimulation sites (limited only by fabrication resolution) as well as simplified fabrication (essentially complete following the automated semiconductor fabrication).

Of concern, however, is the fact that the subretinal approach does not facilitate any form of postoperative image processing in compensation for the anticipated loss of processing mechanisms that exist in a healthy retina. This leaves no mechanism for altering the stimulation parameters (amplitude, stimulus duration, and frequency) should it be found that psychophysical perception is improved by variation of any of these parameters. Another concern exists over the ability to control irreversible and potentially hazardous chemical reactions at the electrode/tissue interface — a situation exacerbated by the relatively small electrode surface areas of these devices. Moreover, the long-term stability of the materials utilized in the fabrication and passivation of such a device remains in question owing to the aggressive chemical environment in which the device is implanted. Finally, in order to

function, the incident light must possess sufficient energy to enable the device to deliver sufficient electrical charge to evoke a physiological response. Without supplemental power, the necessary energy levels of the incident light may be impractical. These concerns notwithstanding, there is no convincing evidence either way as to which stimulation approach (epiretinal or subretinal) is most effective in conveying visual data to a blind human. Therefore, at this early stage in the development of a retinal stimulator, the subretinal approach should not be discounted.

In contrast to the subretinal approach, the epiretinal stimulators being developed generally utilize some form of external power supply to drive and configure the implant. Stimulating electrodes are placed at the vitreoretinal interface. A handful of centers are investigating various designs, each with their own unique attributes. An epiretinal stimulating prosthesis is being developed by a consortium of centers in Germany led by Eckmiller from the University of Bonn [11]. Humayan, de Juan and their co-workers at Johns Hopkins University are developing a prosthesis in collaboration with Liu’s electronics group at the University of North Carolina [12]. Wyatt and Rizzo of Massachusetts Institute of Technology and Harvard, respectively, have proposed a laser-powered system [13]. Yagi and his colleagues of Nagoya University in Japan [14] are proposing a hybrid approach, combining the photodiode array as input but with epiretinal surface electrodes.

The authors’ proposal also utilizes an epiretinal device with the roots of this approach being with the tried and proven technology utilized in cochlear neuroprostheses [15], [16] although with several times more stimulation sites and a unique electrode multiplexing system. The authors have chosen the epiretinal approach primarily due to the concerns expressed in the foregoing paragraph on subretinal prostheses and the authors’ desire to maintain control over the stimuli through an external programming system.

A number of other circuits have been proposed and designed for both research and commercial use in neurostimulation (not limited to retinal stimulation). These include the notable examples of an eight-channel stimulator for the deaf by Hochmair and Hochmair-Desoyer [15], the Nucleus 22-channel hearing prosthesis [16], and the University of Utah’s eight-channel example of a proposed demultiplexing system [17]. These examples utilize some form of trans-tissue telemetry system in their operation, as is the case in the present study. However, none of these have the combined features of 100 stimulation channels, scaleable current output, bidirectional (feedback) telemetry, and intrinsic error-detection mechanisms to ensure patient safety.

II. METHODS

A. System Overview

To place the ASIC within the appropriate context by identifying its role in the overall vision prosthesis system, Fig. 1 describes the general operation. An image is captured from the visual environment by means of a CMOS camera (VV6300, VLSI Vision Limited, UK). The image is processed in the external image processor (StrongARM 1100, Intel, USA) wherein the appropriate attributes of the image, as determined by a programmable protocol, are detected, extracted and pixelized into

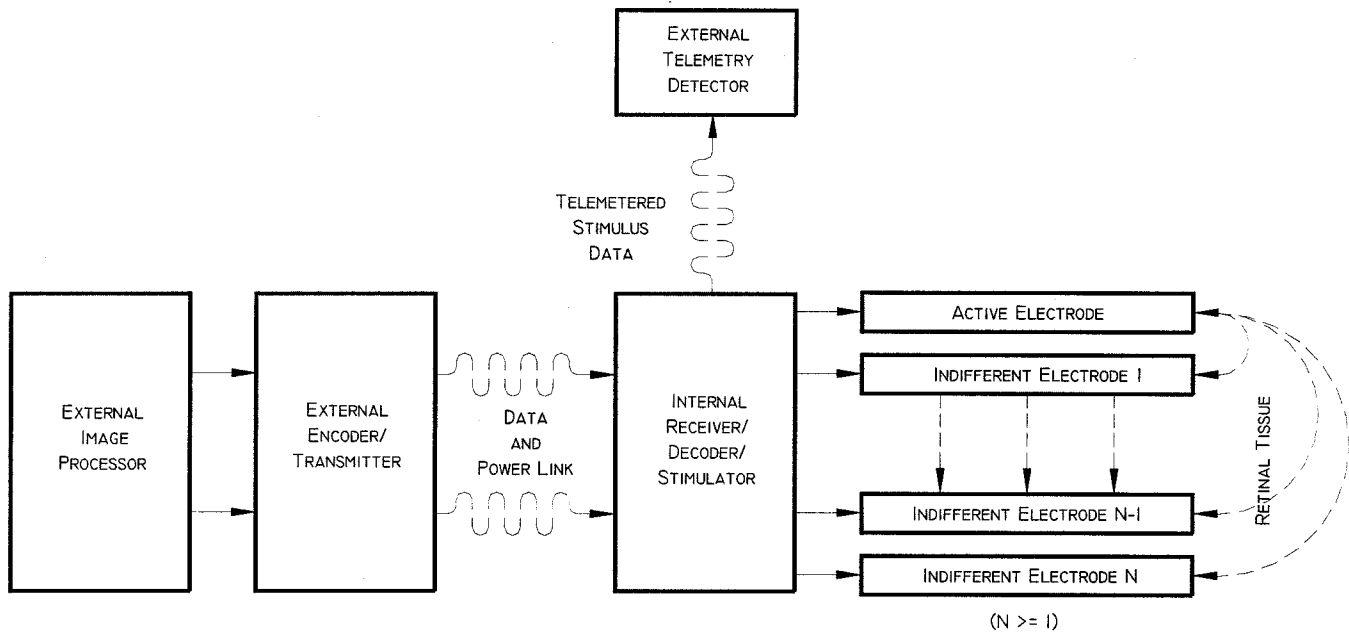


Fig. 1. Block diagram of system operation. External image processor takes in an image from the environment. Image is pixelized according to a programmable compression protocol. External Encoder/Transmitter translates the pixelized image into a series of encoded RF sequences according to a programmable stimulation protocol. RF sequences are broadcast through the ocular tissue via the Data and Power Link. Implanted Receiver/Decoder/Stimulator receives the RF sequences, decodes the data and delivers stimulus from an active electrode, through the neural tissue and returning to an indifferent electrode. Telemetered stimulus data (the end-of-phase voltage across the current source) is detected externally by way of monitoring the transmitting antenna.

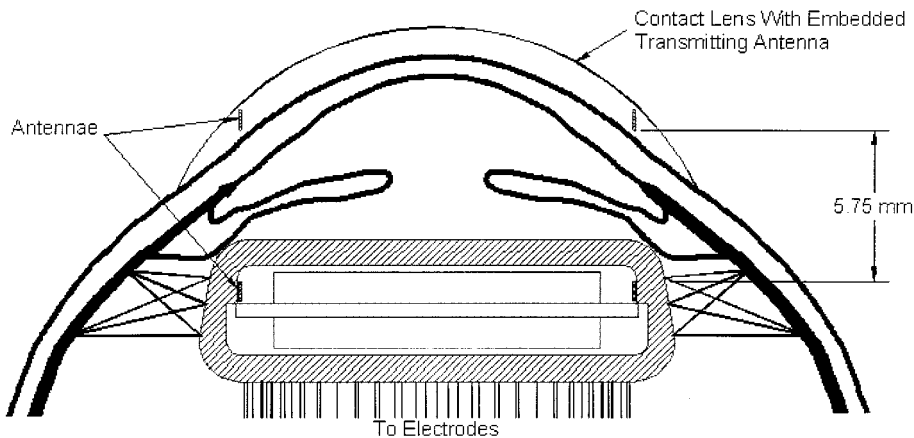


Fig. 2. *In situ* configuration. Anterior chamber and part of the posterior chamber of the eye with scale dimensions typical of the ovis aries. Placed upon the cornea is a transmitting antenna embedded within a permeable contact lens. Within the posterior chamber, the prosthesis is shown encased within a hermetic capsule that is fixed in position by permanent sutures suspended from the sclera. Separation between the transmitting and receiving antennae is 5.75 mm.

a 10×10 array. Within the external encoder/transmitter, each pixel above a selected threshold intensity is translated into an encoded RF telemetry sequence, wherein the active and indifferent electrode(s) selection, current amplitude, stimulus durations (one for each phase of the biphasic waveform) and inter-phase gap duration are encoded. The RF sequence is then broadcast at the carrier frequency (2.5 MHz during testing presented herein) through the ocular tissue to the implanted prosthesis as shown in Fig. 2.

Upon completion of the delivery of stimulus, a request can be made (by extending the period before the next RF sequence) to transmit the end-of-phase voltage as measured across the stimulus circuit. This voltage is transmitted by the implanted pros-

thesis using "reverse telemetry" wherein an energy burst, related in time to the voltage, is broadcast out of the body.

The ASIC was designed in a single iteration on a budget of less than US \$5000 (in addition to the designer salary that formed part of a Ph.D. degree project). The public domain software packages MAGIC, SPICE, and IRSIM were used for the layout of the ASIC, analog modeling and digital simulations, respectively. All of these were run on the Linux operating system using an AMD 6×86 processor platform. Fabrication of the ASIC using the ORBIT 2- μ m technology was contracted through the MOSIS service at the University of Southern California (Los Angeles). The resulting device is shown in Fig. 3.

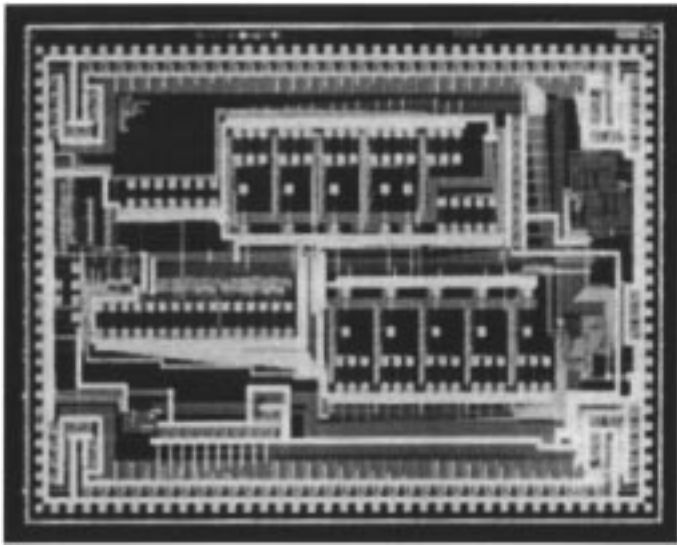


Fig. 3. Micrograph of the ASIC: Die size is 4.6×6.8 mm CMOS fabrication using the $2 \mu\text{m}$ Orbit process.

The block diagram shown in Fig. 4 describes the operation of the ASIC and its peripheral components and is relevant to the following text.

B. RF Power and Data

While the emphasis of the present paper is to describe the ASIC, some discussion of the RF data and power transmission (or RF link) is warranted. A thorough review of this topic is provided in Donaldson and Perkins [18].

The *in situ* configuration of the RF link is as shown in Fig. 2. The authors have chosen the ovis aries (sheep) species as the animal model for surgical fixation and physiological studies. As such, relative dimensions shown in Fig. 2 are relevant to the anatomy of that species.

The transmitting antenna is a 13.4 mm diameter coil, consisting of five turns of 0.125-mm-diameter copper wire. Inductance of the antenna is $1.22 \mu\text{H}$ and is tuned to parallel resonance at 2.5 MHz with a capacitance of 3.33 nF.

Connection of the resonant circuit to a $\pm 5\text{-V}$ supply is gated via a pair of complementary power MOSFETs with data signals from the image processing hardware in accordance with the aforementioned data protocol.

The receiving antenna is also 13.4 mm in diameter so as to fit within the anatomy of an implantable, hermetic capsule (Fig. 2). The antenna consists of six turns of 0.125-mm-diameter copper wire and has an inductance of $1.41 \mu\text{H}$. The circuit is tuned to parallel resonance at 2.5 MHz with 2.88 nF of capacitance. The schematic shown in Fig. 5 describes the data and power extraction used.

C. Data Integrity Protocol and ASIC Programming

In the interest of safety and to ensure the predictable delivery of stimuli to the retinal tissue, the system employs a twofold strategy of data integrity for the delivery of stimulus configuration data.

First, there exist no “preset” parameters in the operation of the system. By setting a fixed phase duration or current amplitude at

the time of system start-up, obvious bandwidth savings may be realized by not having to send this information with each stimulus sequence. However, subsequent corruption of the “preset” parameter(s) resulting from any number of extraneous RF sources is likely to allow potentially harmful or painful stimuli to continue until the system is reset. The authors’ approach is to require each stimulation sequence to reset and reconfigure the implanted prosthesis entirely. This ensures that no erroneous stimulation pulses are delivered on more than one occasion owing to a single event of data corruption. The trade of bandwidth for safety in this instance is necessary in order to avoid the unacceptable consequences of the “preset” corruption scenario.

Second, the stimulation data translation for each RF sequence follows a predetermined safety protocol such that errors may be detected by the ASIC and appropriate remedial action taken in this event.

The DATA signal (Fig. 5) extracted from the RF carrier is “cleaned-up” by passing through a filtering circuit on the ASIC. This signal is then decoded by the ASIC according to the protocol as described below.

Each event of stimulation is configured and delivered by a “sequence” of data. Each sequence contains a series of “packet bursts,” each serving to configure particular aspects of the ASIC or, in the case of stimulus delivery, serving to define the duration of the stimulus. A packet burst is defined by the presence of fixed-frequency pulses. Each packet burst has a beginning and an end whereby fixed carrier frequency pulses commence and cease, respectively. Packet bursts are translated from logic level (0–5 V) signals to RF waves prior to broadcast from the external transmitter by way of an oscillating circuit, tuned to the carrier frequency as described above.

Each packet burst is separated in time by a “silent” period or “packet burst gap” wherein no pulses are present. This packet burst gap is necessary in order to provide a distinct separation of packet bursts and to allow for a packet burst detection circuit to become de-asserted. Choice of packet burst gap duration is based upon: the need to deliver sufficient RF to power the implantable electronics, the need to avoid the possibility of overlapping two or more sequential packet bursts and the need to avoid disabling the sequence detection circuit (described below) during a sequence. The packet burst gap may exist in the form of subthreshold RF signals so as to maintain some power supply. The testing presented herein uses the absence of RF during the packet burst gap.

Due to the energy build-up and discharge intrinsic to all oscillating circuits, undershoot and ringing will occur at the beginning and end of a given RF packet burst, respectively. For this reason, counting the exact quantity of pulses exceeding a given threshold is likely to lead to errors. To eliminate the effects of this phenomenon, a *divide by n* strategy is employed. This allows some pulses to be below the threshold and provides a facility for tolerance of ringing. The selection of the value of n is dependent upon several factors such as damping, frequency, threshold, etc. although the authors’ choice of n to be eight was somewhat arbitrary. Prelayout “breadboard” testing provided satisfactory results with a standard CMOS octal divider, and as a result, the octal division was simply carried over to the ASIC without optimization. Reduction of the division constant would

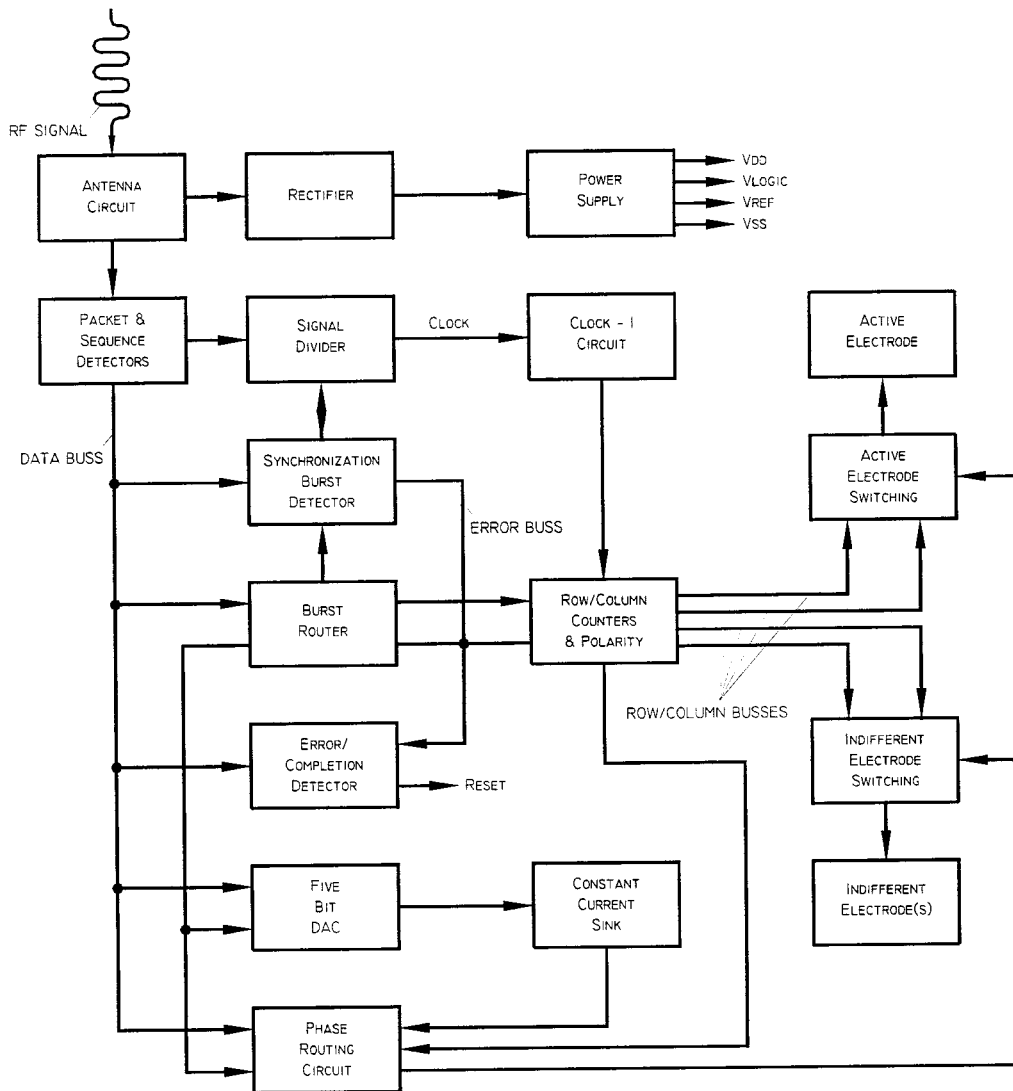


Fig. 4. Detailed ASIC operation. RF energy (received by antenna circuit) is rectified and stored in Power Supply where it is divided and regulated to provide VDD, VLOGIC, and VREF for analog stimulation, digital logic, and reverse telemetry, respectively. Simultaneously, the RF signal passes through packet and sequence detectors then into signal divider for cycle counting and division by eight. These signals are passed to the relevant sub circuits via the data bus. Burst router determines which packet burst of a given sequence is being received, and directs the clock signal to the appropriate module of the circuit accordingly. Initially, synchronization burst detector is activated. An invalid synchronize burst evokes a reset signal from the error/completion detector (via error bus), thus placing the circuit in a state wherein it awaits the next valid synchronize burst. Otherwise, the Burst Router activates the Row/Column Counters & Polarity circuit such that the Row/Column Buses are configured according to the quantity of Clock cycles received. Clock-1 circuit filters the clock signal, subtracting one from the clock signals during each burst. Signals on the Row/Column buses determine which of the Row/Column switches within active and indifferent electrode switching circuits are connected to the output of the phase routing circuit.

provide some (albeit minor) improvement to data throughput although reduction to values less than five would render the data transfer prone to errors. By sending eight RF cycles above a given (logic level) threshold, the implant will count the *packet burst* as: $8/8 = 1$.

Incoming RF cycles are detected by the implant at two levels: packets burst detection and sequence detection. These are "sample and hold" circuits with different resistance-capacitance (RC) time constants.

Upon detection of a packet burst, both detection levels are asserted. Upon the completion of the packet burst, both detection circuits begin to decay while they wait for additional RF cycles to arrive. Packet burst detection waits for approximately 600 ns, slightly longer than the period of the 2.5-MHz carrier fre-

quency, for decay sufficient to de-assert packet detection from logic high to logic low. If no further RF cycles arrive within this time, packet burst detection is de-asserted. The sequence detection circuit waits an extended period of time, approximately 4500 ns, slightly longer than the maximum prescribed packet burst gap, for additional RF cycles to arrive (i.e., the next packet burst). Sequence gaps, being longer than the maximum prescribed packet burst gap, cause the sequence detection circuit to decay and de-assert sequence detection. In effect, the packet burst detection is asserted only when a packet burst is being received whereas sequence detection is asserted throughout the delivery of a sequence.

The errors that are likely to occur during RF transmission would be in the form of either too few or too many RF cycles

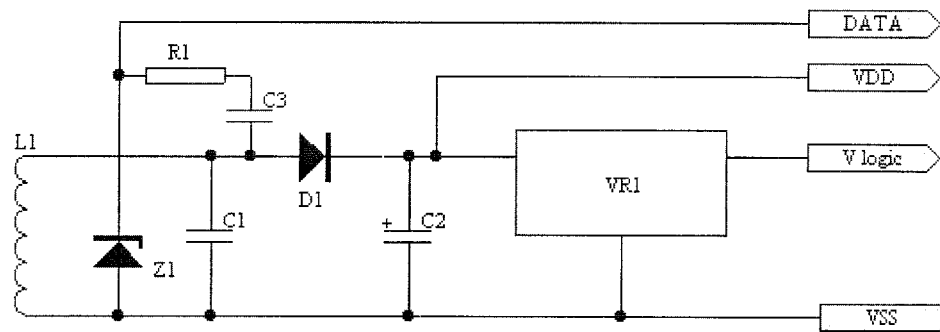


Fig. 5. Power and data extraction circuit. RF is received on inductor (antenna) $L1$ that is tuned to the carrier frequency by capacitor $C1$. Diode $D1$ rectifies the RF and stores charge in capacitor $C2$. Voltage regulator $VR1$ clips the voltage to the desired level for VLOGIC (5 V). Capacitor $C3$ de-couples the RF from the remainder of the circuit such that it may be clipped by zener $Z1$ through resistor $R1$ so as not to introduce supply instability through the ASIC's input protection diodes. Resulting signals include: DATA, the cycles of which are to be analyzed by the ASIC; VDD, unregulated dc for the ASIC's analog stimulation circuitry; VLOGIC, stable supply for logic; and VSS, the lowest potential of the circuit.

through transmission interruptions or extraneous RF. As designed, excess cycles beyond that “allowed” in a given packet burst would trigger an error state in the ASIC and cause a reset. “Lost” cycles would result in the loss of assertion in the sequence detection circuit, thus detecting the error by means other than cycle counting, but nevertheless eventuating a circuit reset. While no specific means exist on the ASIC of detecting deficient or excess RF cycles that remain “valid” from the point of view of simply switching to the “wrong” electrode, errors of this nature would likely be systematic (such as the transmitting antenna becoming displaced). As such, these errors would likely be detected by other means, such as during the synchronize burst for example.

1) *Synchronization*: Each sequence is initiated with a “synchronize burst,” a unique packet burst which alerts the circuit that a sequence is beginning and valid data are to be delivered in subsequent packet bursts. The synchronize burst is unique in comparison to the other packet bursts in that it must be sufficient in duration to assert the packet burst detection circuit but must not have sufficient cycles to trigger a count of one when the cycles delivered are divided by eight. Only by receiving a synchronize burst meeting these conditions will the implant be enabled for decoding subsequent packet bursts. Detection of cycles in excess of seven for a given synchronize burst shall place the implant in a state whereby it is inactive until a new, valid synchronize burst arrives.

2) *Electrode Multiplexing and Current Source Polarity*: Studies by Brindley and Lewin in the late 1960s involved a cortical stimulator comprised of 80 electrodes implanted in the visual cortex of a female volunteer who had developed bilateral glaucoma [19]. Upon application of stimulus, the volunteer reported “seeing” a small spot of white light. The spot was described as “the size of a grain of sago at arm’s length” or “like a star in the sky.”

So as to avoid the infection issues to do with percutaneous connections, the stimulator utilized inductive coupling to deliver stimuli as prescribed from electronics positioned outside the body. Receivers, one per electrode, were implanted beneath the scalp and connected by wire to electrodes positioned within the visual cortex [19]. A “helmet” containing transmitting coils corresponding to each of the implanted receivers was positioned

upon the head of the volunteer. By these means, the visual cortex of the patient could be stimulated.

A significant technological difficulty experienced in this procedure was that of “cross-talk” between the inductive receivers. The cross talk was as a result of misalignment of the transmitter helmet and the small center-to-center distance between the receivers.

In a second study, enhancements to the electronic design by Donaldson produced a “row/column” transmission strategy which dramatically reduced the number of receivers necessary on the implant while maintaining a similar quantity of electrodes (75) [20]. Donaldson’s concept of a row/column solution to Brindley and Lewin’s difficulties also provides a realistic compromise between bandwidth and functionality in the design of a RF telemetry system such as in the present case.

By dividing the 100 electrodes into two distinct blocks of 50 ($A1-50$ and $I1-50$ of Fig. 6), and addressing each member of these blocks by a row and column address, the 100 electrodes may be efficiently and effectively multiplexed to the digital-to-analog converter (DAC) current source. Through utilization of this strategy, the quantity of data passed through the RF telemetry system is dramatically reduced. Using this strategy, any one member of a given electrode block may be stimulated with respect to any one or more member(s) of the opposing electrode block. With some constraint on the stimulus return path (which must pass through one or more electrodes from the opposing electrode block), it is possible to achieve true 100-channel stimulation with minimal set-up data requirements.

A further advantage of dividing the electrodes into two distinct blocks is the ability to place a single capacitor in series with each block ($CAP1$ and $CAP2$ of Fig. 6). This provides an efficient means of dealing with charge imbalances beyond that which may be recovered through application of the biphasic, constant current, waveform as proposed by Lilly *et al.* [21].

Each packet burst in the protocol must exist in its respective order for the circuit to decode the data and avoid protocol violation. In the event that a given packet burst is to achieve nothing (does not turn on any electrode rows or columns), the quantity counted by the circuit using the divide by n strategy must be zero. Since the packet burst must exist, it must contain sufficient cycles to assert packet detection. A packet burst meeting

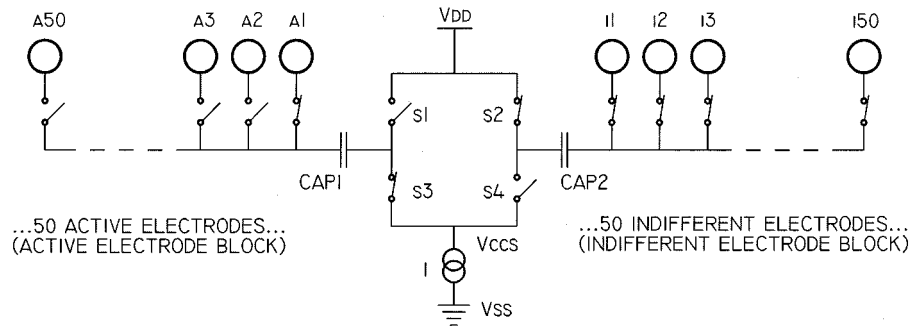


Fig. 6. Electrode switching schematic. Switches $S1$ and $S3$ are simultaneously closed for one phase of stimulus, switches $S2$ and $S4$ are closed for the opposite phase. The 100 electrodes are divided into two distinct blocks, "Active electrode block" and "Indifferent electrode block"; each block comprised of 50 electrodes each. Stimulus passes from one block to the other. Individual electrodes are added to or removed from the stimulation circuit by the closing or opening of their respective switches. Improved recovery of net dc may be achieved through the addition of series capacitors CAP1 and CAP2.

this description would also meet the description of a synchronize burst. In order to differentiate between a synchronize burst and other packet bursts that are delivered to provide a count of $0((8 * 0) + 4 = 4)$, the ASIC employs a "count minus one" circuit. The content of all packet bursts that specify electrode rows or columns is subtracted by one.

Thus, the formula for RF cycle quantities in these packet bursts is

$$\text{counts} = 8 + (8j + 4) \quad (\text{RF cycles.})$$

For a count of zero to be detected by the implant in a given packet burst, 12 cycles are sent. This value exceeds that of the synchronize burst but the "count minus one" circuit interprets this as zero counts.

Packet bursts that serve to configure rows and columns are deciphered through binary counting of their content. Similarly, the polarity is set in this way as well. The polarity signal serves to transpose the roles of the active and indifferent electrode blocks by directing the cathodic phase of the biphasic stimulus to the indifferent block instead of the active block. This facilitates the use of any of the 100 electrodes as the stimulating electrode in a given sequence.

3) *DAC*: There is intrinsic difficulty in developing a stimulation system for physiological excitation of tissue wherein the appropriate current threshold and modulation parameters are yet to be thoroughly defined. In a typical "chicken-before-the-egg" situation, one must either make assumptions based upon the available data or devise a means of scaling the output characteristics such that the full-scale current output may be adjusted to the appropriate range following ASIC fabrication. The authors have chosen a combination of the two.

There exist a number of factors that will influence the range of stimulation current required of the stimulation system. These include parameters such as electrode size, material, and surface roughness, as well as the proximity of the electrodes to excitable tissue, media impedance, tissue excitability, stimulation pulse width, etc. [22]. As the final form of the electrode/tissue interface is likely to undergo evolutionary development, the ASIC possesses a feature whereby the full-scale output range may be adjusted.

The choice of the maximum full-scale output current in the ASIC has been based, in part, on the results of studies performed by researchers at Johns Hopkins University [7]. In their acute

study, psychophysical observations were made while stimulating the retinas of human subjects using a small electrode pair contained within and directed into position by a cannula. Their results indicate that the stimulation current necessary for evocation of a psychophysical response in patients blinded by retinitis pigmentosa or age related macular degeneration is of the order of 300–800 μA under their test conditions. In this study, however, the geometric separation, configuration and proximity to neuronal tissue of the stimulating electrodes are likely to differ from a stimulating prosthesis in its final form. Furthermore, there exist other stimulation profiles wherein increased current amplitudes could be utilized in conjunction with decreased stimulus duration in order to inject similar charge-per-phase, thus facilitating increased stimulation rates. For these reasons, the authors targeted an output current beyond that of the upper limit of the Hopkins results and chose 2 mA to be the maximum full-scale current output.

The ASIC's DAC is comprised of five bits, each bit a factor of two of the subsequent bit with the LSB corresponding to approximately 65 μA when using the full-scale output.

The choice of a linearly scaled DAC as opposed to a logarithmically scaled DAC was primarily due to the largely undefined threshold and operating current parameters as discussed previously. Stimulus thresholds and the effects of small changes about these thresholds have not been studied in depth. In the absence of these data, some advantage may be had by the use of linear scaling as it provides the same resolution across the full-scale range of the DAC. Should it be determined that small variations of current provide a large variation in the psychophysical perception of "brightness" continued use of linear scaling would be warranted, otherwise, logarithmic scaling may be more appropriate in future designs.

As with the configuration of the electrode rows and columns, the DAC is programmed through binary counting of data received during the amplitude packet burst. The programmed current output of the DAC is reduced by subsequent counts of data. The authors believe that the more likely scenario of data corruption would be with too many rather than too few counts from extraneous RF sources and, thus, this decision was taken from the perspective of safety.

4) *DAC Scaling*: Owing to the paucity of repeatable stimulation threshold data and the numerous factors that will in-

fluence the stimulation parameters, a means of adjusting the full-scale current output range is desired so that the entire range of the DAC may be utilized for stimulation profile variation. Furthermore, adjustment of the full-scale output to a level below that at which potentially uncomfortable or harmful stimulation could occur is desirable from a safety perspective. A facility for this adjustment has been included on the ASIC so that, as the situation warrants, the full-scale output current may be reduced by the introduction of a single resistor to the circuit. This resistor serves to reduce the drain to source current of the five DAC bits, thus reducing the full-scale output and maintaining proportional resolution at all scales [above where the field effect transistors (FETs) are operating in saturation — otherwise the DAC output would be nonlinear but nevertheless predictable].

The scaling feature also eliminates the need for additional ASIC design iterations in order to realize high-resolution DAC adjustment once the appropriate full-scale output current is determined through psychophysical studies.

5) *Stimulus Delivery*: Upon completion of the programming of the ASIC through the delivery of the packet bursts that set electrode rows and columns then DAC amplitude, the delivery of stimulus may begin. The electrode chosen as the stimulating electrode shall receive the cathodic phase of the biphasic stimulus first. The duration of the cathodic phase is defined by the period of assertion of packet burst detection for the packet burst defining the first phase of stimulus and is limited only by the transmitting electronics. The anodic phase of the biphasic stimulus (charge recovery phase) begins with the assertion of packet burst detection for the packet burst defining the second phase of stimulus. Similarly, the duration of the anodic phase is defined by the period of assertion of packet burst detection for the phase two packet burst. In normal operation, it is envisaged that the two phases shall be of equal duration, although this is not a requirement.

D. Reverse Telemetry

Following implantation, the implant's circuitry is no longer accessible by conventional means as there are no wires through which signals may be communicated across tissue. As some degree of communication is desirable, and indeed necessary for diagnostics and research, the ASIC has been designed to deliver two reverse telemetry signals, one for the supply voltage (V_{DD}) and another for the voltage across the constant current sink (V_{CCS}). Each of these signals are in the form of a burst of RF energy caused by briefly short circuiting the implant's power supply across the receiving antenna.

This facility provides a noninvasive means of obtaining data yielding the end-of-phase voltage across the circuit through which a given stimulus pulse has been passed. This information can serve several purposes, including:

System Diagnostics — providing a means of *in situ* confirmation of the integrity of each electrode connection, offering clues toward the determination of fault modes such as electrode short or open circuits.

Tissue Impedance — with knowledge of the programmed current, the end-of-phase voltage will provide a means of estimating the tissue impedance for a given stimulus profile. This

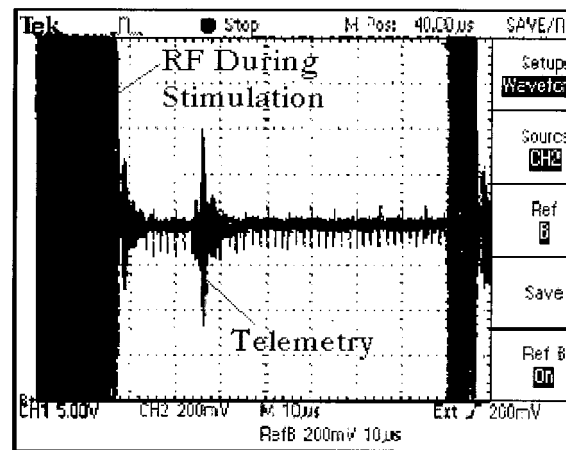


Fig. 7. Reverse telemetry burst.: Time measured from the cessation of RF during stimulation to the onset of the telemetry detection may be translated to the voltage across the constant current source during stimulus.

may yield some insight into the progression over time of fibrous tissue formation at the electrode/tissue interface.

Voltage Waveform Reconstruction — measurement of the end-of-phase voltage for a series of pulse widths will provide data points allowing for the reconstruction of the voltage waveform for a given stimulus amplitude, potentially providing a means of assessing irreversible chemical reactions resulting from stimulus delivery. Following an initial minimum pulse width of approximately $5 \mu\text{s}$ for RF stabilization, resolution in time of the waveform reconstruction is the same as the period of the RF carrier frequency.

A brief “shorting” of the power supply capacitor to the receiving antenna of the implanted prosthesis gives rise to the broadcast of a “spike” of RF energy that is detectable on the transmitting antenna outside the body during the otherwise “silent” period between stimulus sequences (Fig. 7).

Because incoming RF signals would obscure the reverse telemetry signal, it is necessary that a period of RF inactivity exist between successive stimulus sequences in order for the reverse telemetry to be detected. Similarly, the reverse telemetry signal is likely to corrupt the encoded RF signals from the transmitter should the two events occur simultaneously. For these reasons, the telemetry is only delivered when a sufficient gap is present between successive stimulus sequences. In other words, to “turn-on” the reverse telemetry facility, the gap between stimulus sequences is simply extended.

Measuring the time between the end of the second phase of stimulus and the onset of the energy spike provides a means of determining the original value of a voltage that has decayed exponentially (using an RC circuit) to a reference voltage. Said reference voltage is approximately 0.5 VDC and obtained by a voltage divider of the V_{LOGIC} supply. At the time when the measured voltage has decayed to the reference voltage, a voltage comparator initiates the shorting of the power supply capacitor to the implant's antenna ($C2$ and $L1$ of Fig. 5, respectively) for a period determined by a monostable. By connecting the circuit node corresponding to the voltage across the constant current source to the telemetry circuit at the time of stimulus delivery, the subsequent delay between the end of the stimulus

phase and the onset of the RF energy “spike” yields estimation of the end-of-phase voltage present on that node.

This time measurement (t) may be related back to the signal voltage by the following basic formula:

$$V_K = D * V_{REF} * \exp((t - t_s)/RC)$$

where

D constant voltage division of the signal voltage (V_{DD} or V_{CCS});

t_s comparator’s slew delay;

V_{REF} comparator reference voltage;

RC product of the sizes of the exponential decay components in the implant’s telemetry circuitry;

V_K signal voltage following its passage through a diode and further explained in the following.

In an effort to simplify the telemetry circuit, avoiding the need for two operational amplifiers on the ASIC, the V_{DD} and V_{CCS} signals are passed to the telemetry circuit via a diode. As the current passing through this diode is very small and of varying magnitude, the change in voltage across the diode must be considered. This relation is as follows:

$$\Delta V_{DIODE} = 0.65 * (1 - \exp(-(\Delta V_{DIODE} + V_K)/\tau))$$

Where ΔV_{DIODE} is the voltage drop across the diode, and τ is the voltage constant describing the exponential behavior of the diode at a given temperature. Note that this must be solved by iteration.

A further consideration in utilizing V_{CCS} and/or V_{DD} with respect to the stimulation circuit, in particular, attempting to measure tissue impedance, is the potentially significant drain to source impedance that each multiplexing FET contributes to the circuit. The impedance of each FET, and its associated voltage drop, is a function of current and gate to source voltage, as well as transistor geometry.

Owing to these considerations, it is far more convenient to characterize the lump-sum effects of the governing factors involved in the reverse telemetry measurement for each current step and determine the time/voltage relation empirically.

E. Testing and Characterization

1) *RF Link Integrity*: Powered by the rectified RF supply, each of the 100 stimulation channels of the ASIC was connected to a light emitting diode (LED) such that the cathodic phase of stimulus passed through the LED. The LEDs were arranged in a ten-row-by-ten-column array such that rudimentary images, text-based characters and symbols could be conveyed and visualized by an observer. The image processing system was configured to deliver a “travelling spiral” pattern on the LED array such that all stimulation channels were utilized in the conveyance of the pattern and systematic data errors would be immediately obvious to an observer by disruptions in the pattern.

Various separation distances between the transmitting and receiving antennae were made by inserting 1-mm-thick glass microscope slides between the two antennae. At each separation distance, V_{DD} and V_{LOGIC} were measured as well as an assessment made of the integrity of the data transmission by way of observing the spiral pattern displayed on the LED array.

2) *Synchronization*: Appropriate synchronize detection is critical to data integrity. To examine the effectiveness of the synchronize burst detection circuit of the ASIC, a series of RF stimulation sequences containing synchronization bursts of increasing cycle quantities were sent to the ASIC. The status of the ASIC’s error handling logic was monitored (through probing the ASIC’s “RESET” data pin) in order to confirm that corruption in the form of extra RF cycles (beyond seven inclusive of ringing) indeed causes the evocation of the error condition.

3) *Data Integrity*: Confirmation of the effectiveness of the data extraction of the ASIC was encompassed within the RF link integrity testing as described above, as the ability to extract the data is required in order to obtain the travelling spiral used in the evaluation. However, the functionality of all error handling mechanisms is not covered in that test.

In order to confirm that excess RF cycles (beyond that allowed in a given packet burst by the “rules” of the protocol) eventuate a circuit reset, the ASIC was sent erroneous RF while the status of the ASIC’s error handling logic (the ASIC’s “RESET” data pin) was monitored. Each packet burst that sets row, column, polarity or DAC amplitude parameters (all packets excepting “synchronization” and the stimulus delivery phases) was tested in this fashion.

4) *DAC Programming*: Successful data decoding culminates with the delivery of a biphasic waveform at the site of the selected electrode and reference electrode(s). Successful decoding of the DAC data and subsequent delivery of the programmed current during stimulus delivery was confirmed by simulating tissue impedance by fixed resistors, 1 and 3.9 k Ω . The stimulus amplitude results were compared with a SPICE model of the circuit.

5) *DAC Current Scaling*: With a series of fixed resistors varying the DAC scaling resistor, the full-scale current output of the ASIC was adjusted and measured. A comparison of measured full-scale output with predictions made using SPICE modeling was performed.

6) *Reverse Telemetry*: Empirical results were generated using nominal DAC current output of 870 μ A and a regulated 5-V supply so as to facilitate correlation between end-of-phase voltage and the time to the telemetry burst.

III. RESULTS AND DISCUSSION

A. RF Power and Data

Determination of the RF link integrity was performed as described in Section II. The RF link performs satisfactorily in the implant scenario identified in Fig. 2. Results are shown in Table I.

Further observations were made for angular displacement with a separation distance of 5 mm. Rotation of 30.5 degrees about a tangential axis could be tolerated without data loss. Similarly, an eccentricity of 4 mm at 5 mm separation could be tolerated without data loss.

Limited optimization has been applied to this aspect of the project to-date, primarily due to the adequate performance of this preliminary design. However, these results should only be construed as proof-of-point rather than a definitive description of

TABLE I

Separation (mm)	V logic	VDD	Data Integrity
0.0	5.0	9.3	No data loss
1.0	5.0	11.2	No data loss
2.0	5.0	12.4	No data loss
3.0	5.0	11.4	No data loss
4.0	5.0	11.0	No data loss
5.0	5.0	7.8	No data loss
6.0	5.0	6.9	No data loss
7.0	5.0	5.4	Some data loss
8.0	4.4	4.4	Some data loss
9.0	3.6	3.6	Frequent data loss

the RF link in its final form. Indeed there exists significant room for improvement. For example, the parallel transmitting circuit passes significant current (160 mA) through the gating MOSFETS and as such, significant efficiency improvement could be achieved through increasing the inductance of the transmitting coil (associated with a similar increase in the receiving coil). Another alternative is a series resonance design for the transmitter such as that described by Donaldson and Perkins [18].

It is interesting to note that data loss occurred prior to V_{LOGIC} dropping below its setting of 5 V. This is an indication that improved selection of capacitor $C3$ and resistor $R2$ of Fig. 5 could conceivably improve the error free data range.

B. Synchronization and "Configuration"

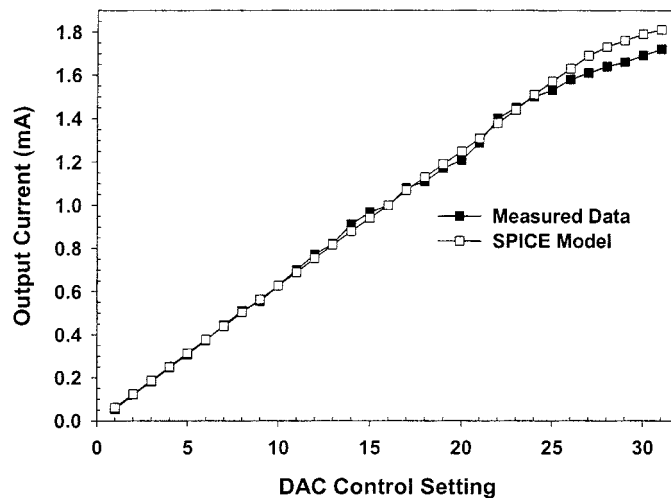
Results of testing described in Section II indicate that the synchronization circuit is performing as designed. Upon detection of cycles contained within the synchronize packet burst in excess of seven, the ASIC enters the error condition and successfully resets itself to await subsequent sequences.

In packet bursts that serve to configure the ASIC (electrode rows, columns, indifferent rows, columns, and DAC polarity and amplitude), RF cycle quantities beyond that "allowed" by the protocol in any packet burst indeed evokes a system reset as designed. Furthermore, sending "constant" RF, as would be the case if there were a transmitter failure in the RF gating circuitry, evokes error detection at the synchronization packet burst and triggers successive circuit resets, never eventuating delivery of a stimulus.

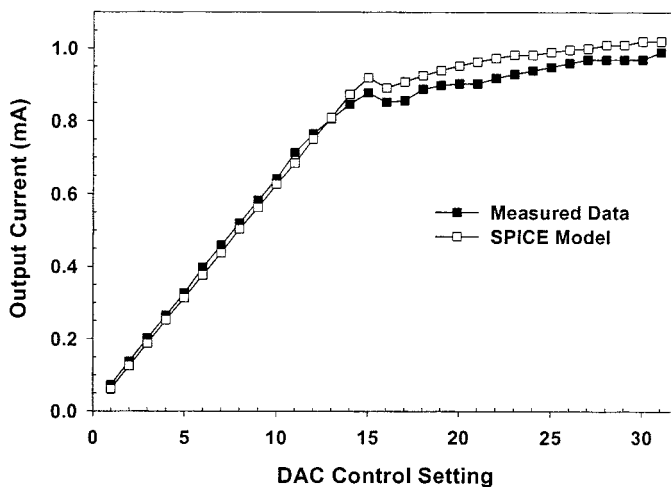
C. DAC Characteristics

Through a 1-kΩ fixed resistor, combinations of the five DAC bits (31 in all) yield good correlation to predicted (SPICE) values. These results are graphed in Fig. 8(a). the moderate nonlinearity toward the upper end of the scale is discussed below.

The ability to achieve the aforementioned full-scale output is affected by a number of factors that influence the observed impedance through which stimulus is passed. As the observed impedance and the device's supply voltage determine the compliance of the constant current DAC at a given amplitude setting, the ability of the prosthesis to achieve this full-scale output current is condition dependent. While the ASIC has been designed to utilize dual supply rails to increase the compliance



(a)



(b)

Fig. 8. DAC characteristics. SPICE estimates in comparison to measured output from the ASIC for simulated loads of (a) 1-kΩ impedance and (b) 3.9-kΩ impedance across the 31 DAC settings.

capabilities of the prosthesis (while maintaining a steady, predictable supply for logic), results presented herein are based upon a single supply rail regulated at 5 V.

As the voltage drop across the tissue impedance increases toward the supply voltage, the ability of the ASIC to supply

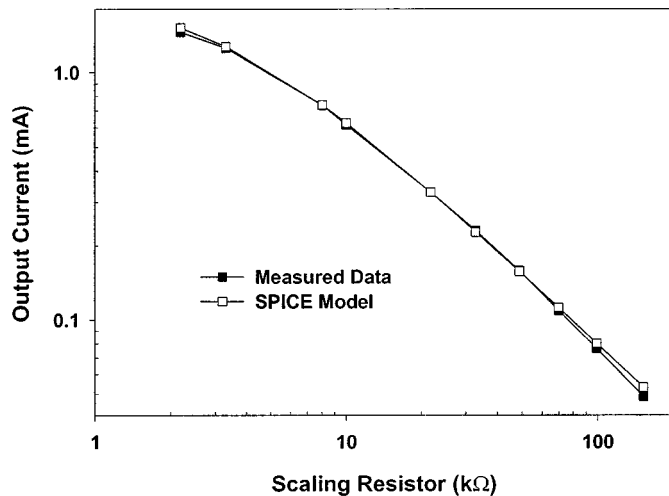


Fig. 9. The effect of the DAC scaling resistor RSCALE. SPICE estimates in comparison to measured output from the ASIC.

additional current is diminished. Simulating tissue impedance by a 3.9-k Ω fixed resistor, SPICE modeling confirms that this is indeed the case. Comparison with results measured using the ASIC is presented in Fig. 8(b).

Fig. 8(b) illustrates an undesirable feature in the circuit design. One would expect that for a 3.9-k Ω impedance and a 5-V supply, that the ASIC would be capable of closely approaching 1.3-mA output current. However, as a result of a design oversight, one of the FETs within the multiplexing circuitry contributes significant impedance (of the order of 1 k Ω) to the stimulating circuit and, thus, limits the output current at the higher DAC settings. This error may be easily rectified in subsequent designs and, can be compensated for in the present design with a moderate increase in supply voltage.

The manner in which the full-scale output is adjusted by variation of the DAC scaling resistor is shown in Fig. 9 wherein both SPICE and measured values from the ASIC are shown.

D. Reverse Telemetry

As an illustrative example of correlation between the stimulus impedance and the time to the telemetry burst, testing was performed for a series of simulated tissue impedances at nominal DAC setting of 870 μ A. These results are provided in Fig. 10. In this study, the results utilize a regulated V_{DD} of 5 V so as to avoid the necessity for two telemetry spikes (the second yielding V_{DD}).

The reverse telemetry facility is essentially a temporally encoded voltmeter. Virtually any circuit node may be connected to the reverse telemetry circuit and broadcast to the outside for deciphering in accordance with the foregoing governing equations (described in Methods). This lends itself to applications for telemetry aside from that of stimulator circuit behavior as has been demonstrated in the Nucleus CI24M cochlear implant wherein reverse telemetry is utilized for evoked auditory potentials (EAP) [23].

E. Stimulation Rate

Attempts to determine the precise site of action potential initiation when electrically stimulating the epiretinal surface have,

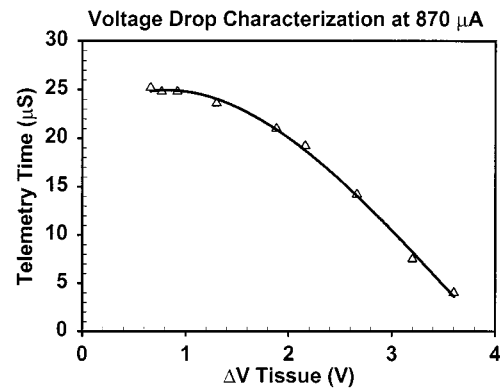


Fig. 10. DAC scaling results: Illustrative example (nominal 870- μ A DAC setting) correlating time to onset of telemetry burst and the change in voltage across the stimulating electrodes. Similar characterizations exist for each of the 31 DAC steps.

thus far, been inconclusive but have nevertheless provoked thought, and increased knowledge in this area significantly. A recent study by Greenberg and his colleagues used a mathematical model in an effort to answer questions raised during their psychophysical studies of human epiretinal stimulation [24]. In particular, they sought to determine: why, when stimulation was applied to a particular region of the epiretinal surface, did the patients perceive a round spot of light rather than a “wedge” of light? A wedge of light would be anticipated if neighboring axons were stimulated in addition to the ganglion cells at the site of stimulation whereas a spot of light would be anticipated if ganglion cell somas were preferentially stimulated over the axons of neighboring cells. Psychophysical studies favor the latter argument [7] as the patients observed (primarily) round spots of light. This argument is backed by some (but not all) of the mathematical modeling leaving the conclusions to be reached by further study.

In the same paper [24], an alternative argument for the reasons behind the psychophysical perception of round spots was proposed. It is possible that the bipolar cells rather than the ganglion cells possess lower stimulation thresholds and as such are the actual site of electrical stimulation. If this is true, some of the processing mechanisms present in a healthy retina remain functional and accessible in damaged retinas. Through selecting the appropriate stimulation parameters (amplitude, frequency and pulse duration), this “higher level” processing mechanism could conceivably be exploited to provide localized phosphenes and, thus, clearer psychophysical images.

From the above discussion, it is clear that the most appropriate form of electrical stimulation is far from being resolved and thus, describing the “stimulation rate” of the present system is a difficult task owing to the number of unresolved factors influencing this concept. In particular, the strategy utilized in conveying the image to the patient will ultimately determine the “stimulation rate.” The system possesses 100 sites of stimulation and therefore it is tempting to describe the rate as the frequency at which an individual site may be stimulated with all other sites being stimulated in series. However, in conveying a meaningful image, it is unlikely that activation of all 100 sites would be beneficial, as the contrast of important features would be reduced by stim-

ulation of surrounding electrodes. The present system possesses two basic mechanisms for the variation of phosphene brightness. Increasing the stimulus charge per phase could conceivably provide phosphene brightness through the recruitment of additional neurons. Frequency modulation may take advantage of temporal summation within the lateral geniculate.

For common return stimulation (one stimulating electrode with the current returning through all 50 electrodes of the opposing block), the average of the setup cycles required (assuming full-scale DAC output) is 588.16 RF cycles. For bipolar stimulation, the average of the setup cycles is 344.32 RF cycles. With a RF carrier frequency of 2.5 MHz, these averages correspond to 235.3- and 137.7- μ s setup time for common return and bipolar stimulation, respectively. As the stimuli are to be delivered in real-time, the duration of the biphasic waveform is simply added to the above values to determine the time required for the complete event of stimulus delivery.

In addition to the stimulation strategy, the “refresh rate” of the 10×10 -pixel array is largely dependent upon the duration of the biphasic waveform. As such, it may be desirable to utilize stimulation strategies wherein these pulse widths are minimized. For example, assuming each phase has duration of 500 μ s, each electrode is stimulated in series, and 50% of the electrodes are stimulated to convey a given image, the “refresh rate” is approximately 19 Hz. Using interleaving as in the conveyance of television images, this refresh rate approaches that of the 25-Hz television refresh rate [50-Hz phase alteration by line (PAL)]. However, as the temporal processing mechanisms present in a healthy retina are by-passed by the electrical stimulation of higher order neurons, the flicker fusion frequency may differ to that of healthy eyes. Humayun and his colleagues have studied the psychophysical effects of epiretinal stimulation on a number of patients [7], [25]. In their recent publication [25], phosphene flicker was eliminated by the application of stimuli at a rate between 40 and 50 Hz. At 19 Hz, the phosphenes generated by electronic stimulation may appear pulsatile, the psychophysical tolerance of which has yet to be determined with compensation anticipated through the enormous processing plasticity of the brain and technological mechanisms that are described below.

Some compelling arguments exist toward maintaining relatively low (tens to hundreds of Hz order) rates of stimulation. Drawing analogies from the wealth of data associated with cochlear neuroprostheses, the more successful speech processing strategies deliver temporal frequency information as amplitude variations at a constant rate of stimulation [26]. In other words, stimulation occurs at a generally fixed rate and tonotopic mapping in conjunction with stimulus current amplitude modulation vary psychophysical perception. Furthermore, the advancing capabilities of the more recent cochlear neuroprostheses, specifically their ability to stimulate at faster rates (kHz order), have raised concern over the ability to recover residual charge imbalances [27] as stimulation rates increase.¹ These examples argue in favor of amplitude modulation over

frequency modulation to convey temporal information. Similar arguments exist with vision prostheses as the traditional mechanisms for charge recovery, namely biphasic waveforms and series capacitors preventing the passage of net DC are common to both fields of neurostimulation.

Increasing amplitude (and, thus, the recruitment of additional neurons) in order to convey brightness in image formation is likely to lead to the perception of larger size phosphenes. These larger phosphenes may limit the benefits of close pitch micro-electrode arrays as the phosphenes generated by adjacent electrodes may overlap. In light of Humayun’s study [25], the ability to increase the frequency of stimulation above that of 19 Hz may be desirable. A conceivable mechanism for increasing the refresh rate is to stimulate in a parallel fashion. At the time of designing the ASIC, this opportunity was considered to be beyond the power supplying capabilities of the RF telemetry. Subsequently, it has been discovered that this is not the case, leaving open the possibility of parallel stimulation as has been achieved in cochlear neuroprostheses [29]. Within certain constraints, the ASIC is capable of parallel stimulation with current division through the stimulating electrodes.

F. Future Improvements

The present system was designed as a tool through which the authors’ physiological and psychophysical studies of epiretinal stimulation may advance and is intended to form a starting point from which more complex and beneficial systems may be derived. The ASIC, designed as part of this system, with its emphasis on patient safety and experimental versatility, remains suitable for its intended purpose. However, as is true with any engineering effort, hindsight provides a means of devising improvements for the future. A few of these examples are presented here.

Parallel stimulation could be controlled further by the addition of multiple DACs on the ASIC. Nine additional DACs could easily be placed within the multiplexing circuitry, thus allowing for multiple electrodes in a given block (active or indifferent) to be stimulated in parallel with identical waveforms. A similar approach has been employed in cochlear neuroprostheses.

An effort was made to anticipate the subsequent mounting of the ASIC within an appropriate hermetically sealed and biocompatible capsule suitable for implantation. As this is to be achieved with similar budgetary constraints as the ASIC development, the method of bonding chosen was “chip-on-board” technology requiring the majority of the bonding pads to exist at the die periphery. Thus, a relatively large die size (4.6×6.8 mm) was utilized to accommodate the 132 pads required for physical connections to the 100 electrodes, supply rails, peripheral components, and desired test points. It is feasible to utilize the identical circuit design and reduce the die size to that of 2.2×2.2 mm using 1.2- μ m technology. The die could then be mounted using “flip-chip” technology so as to avoid the clearance difficulties associated with wire bonding on closely pitched bonding pads.

As mentioned previously, the “ideal” DAC type, logarithmic or linear, remains to be determined. It is desirable to have both types of DAC available on the ASIC with a hard-wired logic bit providing a mechanism for the selection of either DAC.

¹A recent study indicates that charge recovery may be improved through the introduction of a cathodic-anodic-anodic-cathodic stimulus sequence (rather than cathodic-anodic-cathodic-anodic) [28]. However, the effects of this variation on the generation of action potentials, stimulus thresholds and ultimate psychophysical perception are yet to be described in the literature.

IV. CONCLUSION

A 100-electrode neurostimulation ASIC has been designed, fabricated and shown to perform satisfactorily in accordance with the design in terms of DAC output, multiplexing and data decoding via RF telemetry. The system integrates a number of novel features, including 100 unique stimulation sites, bidirectional telemetry, scalable output, programmable DAC, control over pulse widths, and a data transfer protocol with error handling features that ensure patient safety.

The system was primarily designed as part of an intra-ocular vision prosthesis for epiretinal stimulation. However, the telemetry system and stimulus output of the ASIC are such that the system could conceivably be utilized in many other fields of neurophysiology such as stimulation of motor neurons, auditory prosthetics, and bladder control to name but a few.

The advent of this ASIC shall now provide a basis for further research in neurostimulation, specifically, study related to the implementation of intra ocular vision prostheses.

REFERENCES

- [1] G. J. Suaning, N. H. Lovell, K. Schindhelm, and M. T. Coroneo, "The bionic eye (electronic visual prosthesis): A review," *Aust. NZ J. Ophthalmol.*, vol. 26, pp. 195–202, 1998.
- [2] C. Veraart, J. Delbeke, M. C. Wanet-Defalque, A. Vanlierde, J. D. Legat, and C. Trullemans, "Chronic electrical stimulation of the optic nerve in a retinitis pigmentosa blind volunteer," *Invest. Ophthalmol. Vis. Sci.*, vol. 40, p. S783, 1999.
- [3] J. L. Stone, W. E. Barlow, M. S. Humayun, E. de Juan Jr., and A. H. Milam, "Morphometric analysis of macular photoreceptors and ganglion cells in retinas with retinitis pigmentosa," *Arch. Ophthalmol.*, vol. 110, pp. 1634–1639, 1992.
- [4] M. S. Humayun, M. Prince, and E. de Juan Jr. *et al.*, "Morphometric analysis of the extramacular retina from postmortem eyes with retinitis pigmentosa," *Invest. Ophthalmol. Vis. Sci.*, vol. 40, pp. 143–148, 1999.
- [5] G. J. Suaning and N. H. Lovell, "A 100-channel stimulator for excitation of retinal ganglion cells," presented at the 20th Annu. Int. Conf. IEEE Engineering in Medicine and Biology Society, Hong Kong, China, Oct. 28–Nov. 1 1998.
- [6] G. S. Brindley, "The site of electrical excitation of the human eye," *J. Physiol.*, vol. 127, pp. 189–200, 1955.
- [7] M. S. Humayun, E. de Juan Jr., G. Dagnelie, R. J. Greenberg, R. H. Propst, and D. H. Phillips, "Visual perception elicited by electrical stimulation of retina in blind humans," *Arch. Ophthalmol.*, vol. 114, pp. 40–46, 1996.
- [8] A. Y. Chow and V. Y. Chow, "Subretinal electrical stimulation of the rabbit retina," *Neurosci. Lett.*, vol. 225, pp. 13–16, 1997.
- [9] G. Peyman, A. Y. Chow, C. Liang, V. Y. Chow, J. I. Perlman, and N. S. Peachey, "Subretinal semiconductor microphotodiode array," *Ophthalmic Surg. Lasers*, vol. 29, pp. 234–241, 1998.
- [10] E. Zrenner, K. D. Miliczek, and V. P. Gabel *et al.*, "The development of subretinal microphotodiodes for replacement of degenerated photoreceptors," *Ophthalmic Res.*, vol. 29, pp. 269–280, 1997.
- [11] R. Eckmiller, "Learning retina implants with epiretinal contacts," *Ophthalmic Res.*, vol. 29, pp. 281–289, 1997.
- [12] W. Liu, E. McGucken, M. Clements, S. C. DeMarco, K. Vichienchom, C. Hughes, M. Humayun, E. de Juan, J. Weiland, and R. Greenberg, "An implantable neuro-stimulator device for a retinal prosthesis," in *International Solid-State Circuits Conference*, Feb. 1999, pp. 216–217.
- [13] J. Rizzo, M. Socha, D. Edell, B. Antkowiak, and D. Brock, "Development of a silicone retinal implant: Surgical methods and mechanical design," *Invest. Ophthalmol. Vis. Sci.*, vol. 34, p. 1535, 1994.
- [14] T. Yagi, N. Ito, M. Watanabe, T. Matsushima, and Y. Uchikawa, "A study on hybrid artificial retina with cultured neural cells and semi-conductor micro-device," in *Proc. 1998 IEEE Int. Joint Conf. Neural Networks (IJCNN'98)*, pp. 780–783.
- [15] E. S. Hochmair and I. J. Hochmair Desoyer, "An implanted auditory eight-channel stimulator for the deaf," *Med. Biol. Eng. Comput.*, vol. 19, pp. 141–148, 1981.
- [16] P. A. Crosby, P. M. Seligman, and J. F. Patrick *et al.*, "The nucleus multi-channel implantable hearing prosthesis," *Acta. Otolaryngol. Suppl. (Stockh)*, vol. 411, pp. 111–114, 1984.
- [17] K. E. Jones and R. A. Normann, "An advanced demultiplexing system for physiological stimulation," *IEEE Trans. Biomed. Eng.*, vol. 44, pp. 1210–1220, Dec. 1997.
- [18] N. Donaldson and T. Perkins, "Analysis of resonant coupled coils in the design of radio frequency transcutaneous links," *Med. Biol. Eng. Comput.*, vol. 21, pp. 612–627, Sept. 1983.
- [19] G. S. Brindley and W. S. Lewin, "The sensations produced by electrical stimulation of the visual cortex," *J. Physiol. (Lond)*, vol. 196, pp. 479–493, 1968.
- [20] P. E. K. Donaldson, "Experimental visual prosthesis," *Proc. IEE.*, vol. 120, pp. 281–298, 1973.
- [21] J. C. Lilly, J. R. Hughes, E. C. Alvord Jr., and T. W. Galkin, "Brief, noninjurious electric waveform for stimulation of the brain," *Science*, vol. 121, pp. 468–469, 1955.
- [22] L. S. Robblee and T. L. Rose, "Electrochemical guidelines for selection of protocols and electrode materials for neural stimulation," in *Neural Prost. Fundamental Studies*, W. F. Agnew and D. B. McCreery, Eds. Englewood Cliffs, NJ: Prentice-Hall, 1990, pp. 26–66.
- [23] C. J. Brown, P. J. Abbas, and B. J. Gantz, "Preliminary experience with neural response telemetry in the nucleus CI24M cochlear implant," *Amer. J. Otol.*, vol. 19, no. 3, pp. 320–327, May 1998.
- [24] R. J. Greenberg, T. J. Velte, M. S. Humayun, G. N. Scarlatis, and E. De Juan Jr., "A computational model of electrical stimulation of the retinal ganglion cell," *IEEE Trans. Biomed. Eng.*, vol. 46, pp. 505–514, May 1999.
- [25] M. S. Humayun, E. de Juan Jr., J. D. Weiland, G. Dagnelie, S. Katona, R. J. Greenberg, and S. Suzuki, "Pattern electrical stimulation of the human retina," *Vis. Res.*, vol. 39, no. 15, pp. 2569–2576, July 1999.
- [26] G. M. Clark, "Electrical stimulation of the auditory nerve: the coding of frequency, the perception of pitch and the development of cochlear implant speech processing strategies for profoundly deaf people," *Clin. Exp. Pharmacol. Physiol.*, vol. 23, pp. 766–776, 1996.
- [27] C. Q. Huang, R. K. Shepherd, P. M. Carter, P. M. Seligman, and B. Tabor, "Electrical stimulation of the auditory nerve: direct current measurement *in vivo*," *IEEE Trans. Biomed. Eng.*, vol. 46, pp. 461–470, Apr. 1999.
- [28] C. Q. Huang, R. K. Shepherd, and P. M. Carter, "Electrical stimulation of the auditory nerve: pH changes *in vivo* and *in vitro*," in *Proc. 20th Aust. Neurosci. Soc.*, vol. 11, 2000, p. 216.
- [29] B. S. Wilson, C. C. Finley, D. T. Lawson, R. D. Wolford, D. K. Eddington, and W. M. Rabinowitz, "Better speech recognition with cochlear implants," *Nature*, vol. 352, no. 6332, pp. 236–238, July 1991.



Gregg Jørgen Suaning was born in the San Francisco area of California. He received the B.Sc. in 1986 and the M.Sc. in 1988, both in mechanical engineering from the California State Universities at Chico and San Jose, respectively. He is now working toward the Ph.D. degree in the Graduate School of Biomedical Engineering, University of New South Wales, Sydney, Australia.

Upon moving to Australia in 1991, he became involved in the research and development of implantable cochlear neuroprosthesis for the profoundly deaf and severely hearing impaired. His field of study is in prosthesis design and the electrophysiology associated with retinal neuralprostheses.



Nigel H. Lovell (M'91–SM'99) received the B.E. (Hons.) and Ph.D. degrees from the University of New South Wales (UNSW), Sydney, Australia.

He is currently a Faculty Member of the Graduate School of Biomedical Engineering at UNSW. His research work has been multidisciplinary; covering areas of expertise ranging from Web-enabling technologies, database design, biomedical instrumentation, biological signal processing, cardiac neurophysiology, and physiological modeling.

Dr. Lovell is currently the IEEE Engineering in Medicine and Biology Society (EMBS) Webmaster and Chairs the committee on Information Technology Infrastructure. He is a member on the Administrative Committee of the EMB Society (2000–2002). He was recently awarded the IEEE Millennium Medal for services to the EMBS in relation to its Web-based infrastructure.